PAPER

Check for updates

Enhanced fluorescence properties of terbium complex/poly-L-lactic acid superfine fibers sensitized by the LSPR effect of silver nanoparticles†

Shipeng Wen, [ID] [a] Guiming Zhang,[a] Rong Zhang,[a] Liqun Zhang[a] and Li Liu*[ab]

In this research, Ag-NPs/Tb-complex/PLLA composite fibers with diameters of around 250 nm were successfully obtained by the electrospinning and characterized by scanning electron microscope (SEM), transmission electron microscopy (TEM), X-ray photoelectron spectroscopy (XPS) and fluorescence spectra. The influence of localized surface plasmon resonance (LSPR) of silver nanoparticles (Ag-NPs) on the fluorescence of Tb(acac)$_3$phen/poly-L-lactic acid (Tb-complex, acac = acetylacetone; phen = phenanthroline, PLLA = poly-L-lactic acid) fibers was mainly investigated. It is found that Tb-complex dispersed in the fibers in the form of nanoclusters. The local field surrounding of Tb^{3+} ions was affected by the neighboring Ag-NPs. As a result of the LSPR effect of Ag-NPs, the fluorescence intensity, quantum efficiency of Tb-complex in the composite fibers with the Ag/Tb ratio of 4 : 1, were simultaneously improved compared with the composite fibers without Ag-NPs.

Introduction

Fluorescence nanofibers have attracted growing interest because of the potential applications in biological fields such as skeletal muscle tissue engineering,[1] bio-imaging,[2] drug carriers,[3] and fluorescent probes.[4] Traditional fabrication methods of fluorescence fibers mainly include solution spinning and melting spinning. Nevertheless, both of them can barely obtain the fibers with diameters below 500 nm. In recent decades, electrospinning as a universal and effective method for fabricating uniform ultrafine fibers has exhibited many advantages, such as small diameters ranging from tens to hundreds of nanometers,[5] high porosity, large specific surface area,[6] large length to diameter ratios, and good uniformity.[7] Also, electrospinning is a direct method of generating composite nanofibers containing luminescent agents with uniform dispersion.[8] At present, many researchers have prepared fluorescence nanofibers *via* electrospinning. For instance, Zhang *et al.*[9] prepared efficient luminescent Eu(TTA)$_3$phen/polystyrene (TTA = 2-thenoyltrifluoroacetone, phen = 1,10-phenanthroline) nanofibers with diameters ranging from 350 to 700 nm by electrospinning. Huang *et al.*[10] prepared Eu(DBM)$_3$phen/polystyrene (DBM = dibenzoylmethane) fluorescence composite fibers with

diameters of around 300 nm through electrospinning. The energy transfers from phen and DBM to Eu^{3+} ion were very efficient. The Eu^{3+} ions were located in a highly polarizable chemical environment, and this was beneficial to the fluorescence lifetime and internal quantum efficiency of the fibers. Gai *et al.*[11] fabricated Fe$_3$O$_4$/PVP//Tb(BA)$_3$phen/poly(vinyl pyrrolidone) (BA = benzoic acid) magnetic-photoluminescence bifunctional nanofibers by employing a parallel axial electrospinning setup. The average diameter of the individual fiber was around 200 nm. The nanofiber bundles exhibited strong green emissions under the excitation of 275 nm.

It is known that the localized surface plasmon resonance (LSPR) effect is an optical phenomenon generated by collective oscillations of electron gas in metal nanostructures surrounded by a dielectric.[12] As a typical material for plasmonic applications, silver displays sharp and intense LSPR bands.[13] When the frequencies of incident light and the free electron collective oscillation are same, resonance can be produced.[14] Adsorption of molecules on the metal surface lead to measurable spectral changes in both the wavelength and intensity of the LSPR.[15,16]

Surface plasmon resonance-enhanced fluorescence (SPREF) phenomenon of rare-earths/Ag hybrid can be generated when rare-earth particles are close to the Ag particles (Ag-NP) within a few nanometers.[17–19] With the irradiation of visible light, the LSPR of Ag particles can be excited. The LSPR effect results in an enhanced electromagnetic radiation field and thus increases the emission intensity of rare-earth particles in the vicinity of the Ag particles.[20,21] Previous research has confirmed that Ag-NP acts as an effective enhancement agent.[22,23] Lin *et al.*[24] prepared

[a]Beijing Engineering Research Centre of Advanced Elastomers, Beijing University of Chemical Technology, Beijing 100029, China. E-mail: liul@mail.buct.edu.cn

[b]State Key Laboratory of Chemical Resource Engineering, Beijing University of Chemical Technology, Beijing 100029, China

† Electronic supplementary information (ESI) available. See DOI: 10.1039/c7ra02401k

Pb/Cd-free oxyfluoride glasses, and then introduced molecular-like (ML) Ag clusters with 1–4 nm into the glasses. The results demonstrated that the energy transfer from ML-Ag clusters to Tb^{3+} and Yb^{3+} led to the enhancement of near infrared (NIR) emission intensity of Yb^{3+} ions. Hayakawa et al.[25] prepared SiO_2 glass containing Ag^+ and Eu^{3+} ions by annealing the glass in a reducing atmosphere. The results showed that an induced surface plasma oscillation by incidence and an interaction between Eu^{3+} and Ag particles occurs simultaneously. The fluorescence of Eu^{3+} was enhanced in the presence of silver particles with the size of 4.3 nm. Zhang et al.[26] prepared an Ag co-doped SiO_2 (SiO_2:Tb^{3+}–Ag) nanostructured luminescent composite using a modified Stöber method. The results showed that Ag nanoparticles greatly enhanced the light absorption at 226 nm and the light emission at 543 nm of the composite, and the fluorescence lifetime reduced with the increase of Ag concentration in SiO_2:Tb^{3+}–Ag composite.

In this research, the main objective is to prepare superfine fibers with strong fluorescence properties in the presence of Ag nanoparticles. Hence, terbium complex $Tb(acac)_3phen$ (Tb-complex) emitting a strong green light, and Ag-NPs were introduced into poly-L-lactic acid (PLLA) matrix. Finally, the PLLA superfine fibers containing Ag-NPs and Tb-complex were prepared by electrospinning. The diameter of the composite fibers was around 250 nm. Tb-complex had a fine dispersion in the PLLA fibers. The fluorescence intensity of fibers at 539 nm was greatly enhanced by Ag-NPs when the mole ratio of Ag and Tb-complex was 4 : 1. The composite fibers displayed higher quantum efficiency and longer fluorescence lifetime than the composite fibers without Ag-NPs.

Experimental

Materials

Terbium oxide (Tb_4O_7, purity 99.9%) was purchased from Grirem Advanced Materials Co., Ltd (Beijing, China). Silver nanoparticles (Ag-NPs) and polyvinylpyrrolidone (PVP, M_w = 1300 000) were purchased from Sigma-Aldrich Trading Co., Ltd (Shanghai, China). Poly-L-lactic acid (PLLA, M_w = 70 000) was obtained from Guanghua Weiye industrial Co., Ltd (Shenzhen, China). Acetylacetone (acac), phenanthroline (phen), dichloromethane (DCM), N,N-dimethyl formamide (DMF), nitric acid (HNO_3), and anhydrous ethanol (C_2H_5OH) are all commercial reagents.

Synthesis of $Tb(acac)_3phen$ (Tb-complex)

$Tb(NO)_3$ was obtained through the reaction of Tb_4O_7 and HNO_3. 0.1 mol of $Tb(NO)_3$ was dissolved in C_2H_5OH. The $Tb(NO)_3$ solution was magnetically stirred until the $Tb(NO)_3$ was dissolved completely. Then, 0.3 mol of acac was first dissolved in C_2H_5OH and this mixture was then added into the $Tb(NO)_3$ solution. After 1 hour, 0.1 mol of phen was dissolved in C_2H_5OH. The phen solution was then added to the $Tb(NO)_3$ solution. 3 hours later, white precipitates gradually appeared. Finally, the precipitate was dried at 60 °C. The production efficiency was 53%. The IR spectra of acac, phen and Tb-complex

are shown in ESI (Fig. S1†). The characteristic peaks of C=O and C–N shift to the new position after the reaction, indicating that Tb^{3+} ions have coordination reactions with the C=O of acac and two nitrogen atoms of phen.

Preparation of Ag-NPs/Tb-complex/PLLA fibers

PLLA was dissolved in DCM, and the resulting solution was magnetically stirred for 12 hours to form solution (I). Tb-complex was dissolved in DMF, and the resulting solution was magnetically stirred for 15 minutes to form solution (II). A certain amount of Ag-NPs and PVP were added to DMF to form solution (III) that was treated under ultrasonic waves for 1 hour. Finally, the solutions of (I), (II) and (III) were mixed together and magnetically stirred for 1 hour. In the mixture solution, the PLLA content was 8 wt% and the Tb-complex content was 5 wt%. The mixture solution was then transferred into an injection syringe and ready to be electrospun into fibers. The parameters of the electrospinning process are listed as follows: the feeding rate was 1.0 ml h^{-1}; the distance from needle to collector was 15 cm; the voltage was 15 kV; the speed of collecting drum was 300–400 rpm. The electrospinning was carried out for 2.5 hours in order to achieve a fiber membrane. Finally, a series of fibers with Ag-NPs/Tb-complex mole ratios of 0, 1, 2, 3, 4, 5, 8 and 10, were prepared separately.

Characterizations

The morphology of fibers was observed by a scanning electron microscope (SEM, S-4800); prior to observation, gold processing for the samples was received and the voltage was set at 1 kV. A transmission electron microscope (TEM, Tecnai G2 F30 S-TWIN) and an energy dispersive X-ray spectroscope (EDS) were used to observe dispersion of Tb-complex and Ag particles in the fibers. An X-ray photoelectron spectrometer (XPS, Escalab 250) was used to detect the contents of Ag and Tb in different areas of the fibers. Excitation and emission spectra of the fibers were obtained from a fluorescence spectrophotometer (F-4500, Hitachi). The scanning speed, sweep voltage and slit width were set at 1200 nm min^{-1}, 400 V and 2.5 nm, respectively. Fluorescence quantum efficiency was obtained from a fluorescence spectrophotometer (F-4700, Hitachi). An integrating sphere method was used to gain the latter's absolute rate. Wavelengths of excitation and emission of Tb-complex and fibers were set at 294 nm and 539 nm, respectively. Neutral Al_2O_3 powders and empty fiber were used as the reference samples for the Tb-complex and fibers, respectively. Fluorescence lifetime was obtained by use of a steady-state and time-resolved fluorescence spectrometer (FLS920, Edinburgh Instruments). The excitation wavelength was set at 294 nm.

Results and discussion

Original morphologies of Tb-complex particles are shown in Fig. 1A. From the inset, it can be seen that Tb-complex particles have a sheet shape. The size of most Tb-complex particles is in the range of 4–6 μm. Fig. 1B shows that Ag-NPs have a spherical shape with diameters of around 30 nm, and are easily
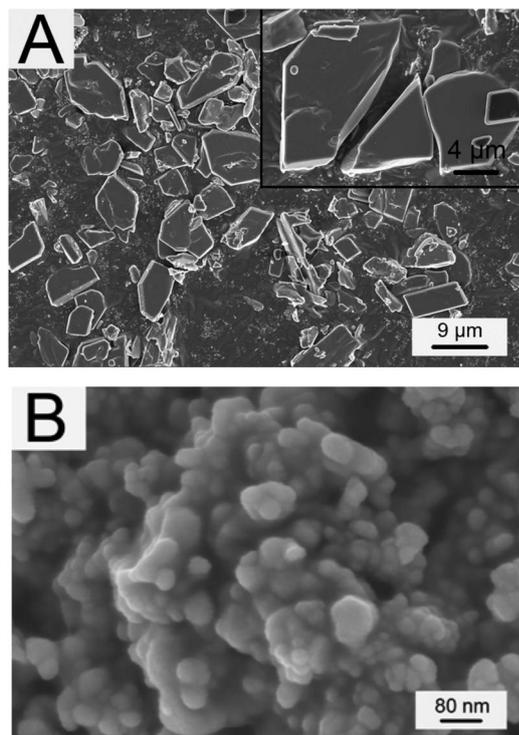
Fig. 1   SEM images of (A) Tb-complex particles and (B) Ag-NPs.

Fig. 2   SEM images of (A) Tb-complex/PLLA fibers, (B) Ag-NPs/Tb-complex/PLLA fibers (Ag : Tb = 4 : 1).

aggregated into a particle of larger dimension (Fig. 1B). Hence, PVP as dispersion agent was added into the Ag electrospun solution before electrospinning to ensure Ag-NPs were well dispersed in the solution.

Fig. 2 shows the morphologies of Tb-complex/PLLA and Ag-NPs/Tb-complex/PLLA fibers. Tb-complex/PLLA fibers have the diameters of about 400 nm and smooth surfaces (Fig. 2A). After Ag-NPs were added into the Tb-complex/PLLA fibers, the diameter of the fibers further decreased to about 250 nm (Fig. 2B). The reason for this decrease in fiber diameter is attributed to the higher charge density on the surface of ejected jet after the addition of Ag-NPs. The increased charge density further results in high elongation forces imposed to the jet under the electrical field. It is known that the overall tension in the electrospun fibers depends on the self-repulsion of the excess charges on the jet. Therefore, the increased charge density of fibers after the addition of Ag-NPs leads to thinner diameter of the fibers.[27–29]

TEM and EDS were further employed to observe the dispersion of Ag-NPs and Tb-complex particles in the fibers. Fig. 3A shows a TEM image of Tb-complex/PLLA fibers. Only some very tiny black dots of Tb-complex particles with the size under 5 nm can be observed in the interior of the fiber. EDS was used to detect Tb contents in different areas. The results show that the contents of Tb in area 1 and 2 are 4.23 and 4.76 wt%, respectively. Compared with the large sheet shape of original Tb-complex particles illustrated in Fig. 1A, the decrease in the size of Tb-complex particles in the fibers can be attributed to particular features of electrospinning process. Before the electrospinning process, Tb-complex was first dissolved in the
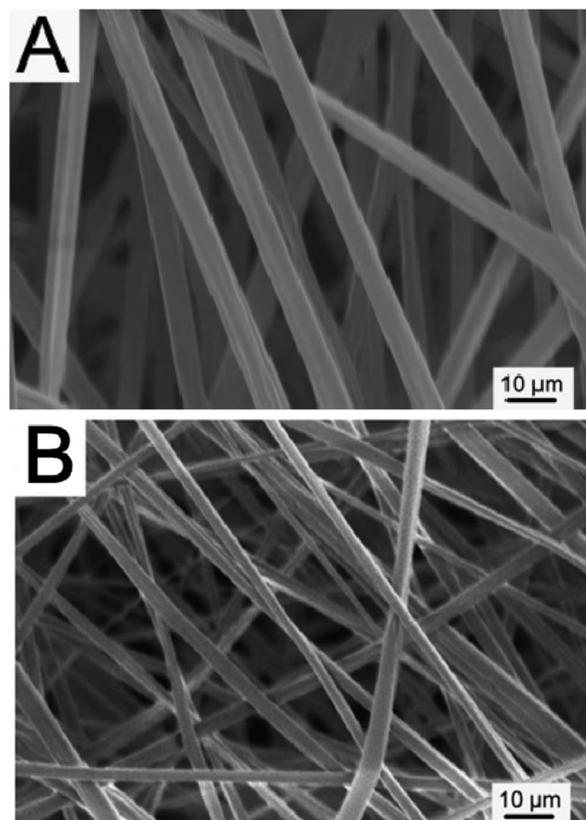
electrospun solutions and existed in the form of single molecule. During the electrospinning process, solvents in the electrospun solution evaporated quickly and the Tb-complex molecules did not have enough time to aggregate into big particles. As a result, most Tb-complex molecules may gather into some nanoclusters in the fibers. Fig. 3B shows the dispersion of Ag-NPs and Tb-complex in the fibers. Ag-NPs of different diameters are incorporated in the fibers such as in the range of 50–80 nm instead of original 30 nm. That is because Ag-NPs are incompatible with PVP molecules, resulting in a certain degree of phase separation between them. Although ultrasonic treatment of Ag solution was employed before electrospinning, Ag-NPs still tended to form aggregates in the composite fibers. EDS detection was further used in a rich Ag-NP area and a blank area. The results show that the contents of Tb^{3+} ions in area 3 and 4 are 3.02 and 2.58 wt%, respectively. This indicates that the addition of Ag-NPs do not affect the dispersion of Tb-complex in the fibers.

XPS was used to investigate the influence of Ag-NPs on the local field surrounding of Tb^{3+} ions in the fibers. The element scans of XPS show that the contents of Tb^{3+} ions in the PLLA and Ag-NPs/Tb-complex/PLLA (Ag/Tb = 4 : 1) fibers are 3.20 and 3.32 wt%, respectively. These results are consistent with those from TEM-EDS tests. In the XPS spectra (Fig. 4.) for Tb-complex/PLLA fibers, both peaks appear at 1245.9 and 1225.1 eV attributed to $3d_{5/2}$ of Tb^{3+} ions. However, the two peaks in the XPS spectra for Ag-NPs/Tb-complex/PLLA fibers shift to a lower
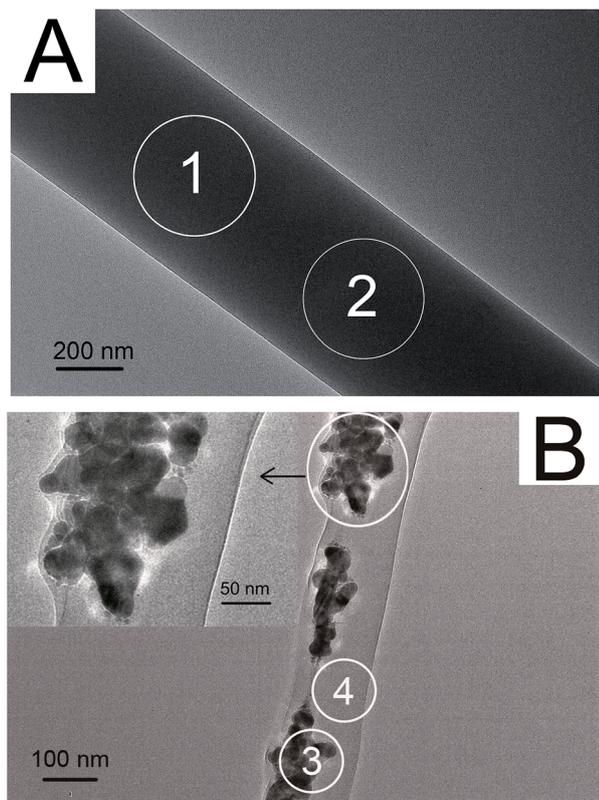
Fig. 3 TEM images of (A) Tb-complex/PLLA fibers containing 5 wt% Tb-complex and (B) Ag-NPs/Tb-complex/PLLA fibers (Ag : Tb = 4 : 1).
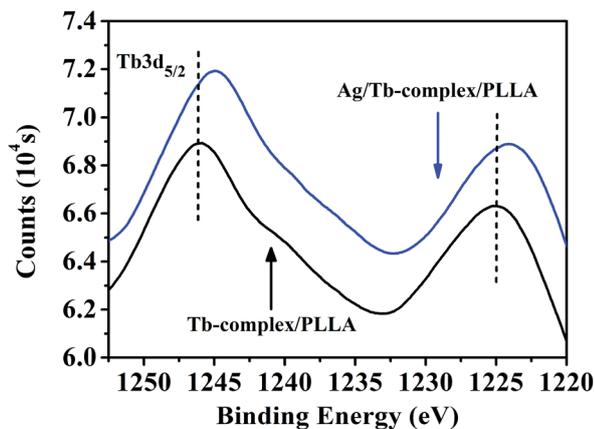

Fig. 4 Binding energy of Tb^{3+} ions in the Tb-complex/PLLA and Ag/Tb-complex/PLLA fibers.

binding energy. This change indicates that Ag-NPs have changed the local field surrounding of Tb^{3+} ions in the fibers.

Fig. 5 shows the excitation and emission spectra of Tb-complex. The excitation spectrum (Fig. 5A) exhibits a platform, revealing that the Tb-complex can be excited by a wide-range light ranging from 325–360 nm. The broad platform is mainly attributed to the wide absorption of organic ligands acac and phen. In the emission spectrum (Fig. 5B), there are four characteristic peaks corresponding to the $^5D_4-^7F_6$ (490 nm),
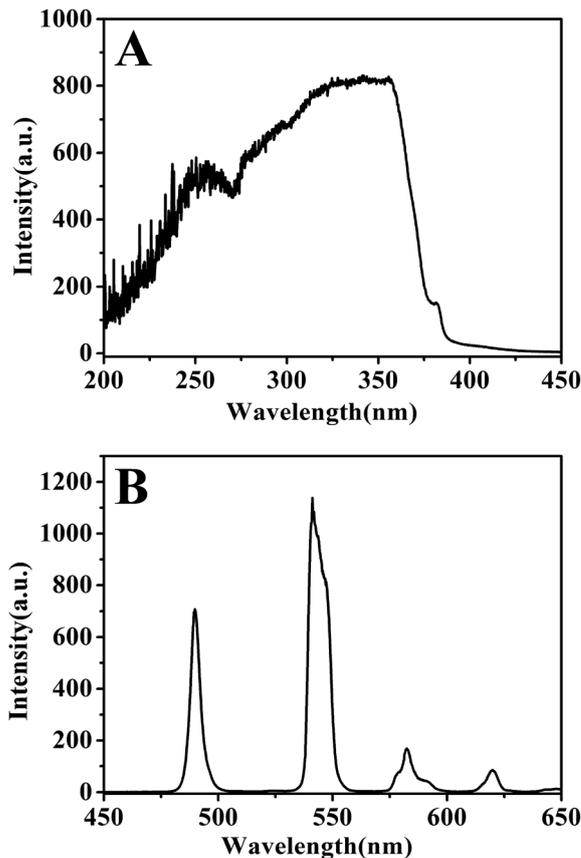

Fig. 5 (A) Excitation (λ_{em} = 541 nm) and (B) emission spectra (λ_{ex} = 351 nm) of Tb-complex.

$^5D_4-^7F_5$ (541 nm), $^5D_4-^7F_4$ (582 nm), $^5D_4-^7F_3$ (620 nm).[30] Among these peaks, the peak attributed to maximum emission intensity appears at 541 nm. Good fluorescence performance is attributed to the high efficient energy transfer from the ligands acac and phen to Tb^{3+} ions.

Fig. 6 shows the excitation and emission spectra of Ag-NPs/Tb-complex/PLLA fibers. It is noted that the broad peaks of Tb-complex in Fig. 5A have blue-shifted, and have been split into two peaks in composite fibers (Fig. 6A). This phenomenon indicates the local field surrounding around Tb^{3+} ions has changed in the fibers compared with that in Tb-complex powders. In the emission spectra (Fig. 6B), all samples show the same fluorescence peaks with Tb-complex illustrated in Fig. 5B. The strongest peak still appears around 541 nm. The fluorescence intensity of fibers is much lower than that of Tb-complex powders. The main reasons for the decreased fluorescence intensity are the low concentration of Tb^{3+} in the fibers and the poor absorption and transfer efficiency of the PLLA matrix. It should be noted that the fluorescence intensity of Ag-NPs/Tb-complex/PLLA fibers is stronger than that of Tb-complex/PLLA fibers. As the content of Ag-NPs in the fibers increases (Fig. 6C), the fluorescence intensity of the composite fibers also increases and reaches the highest value when the mole ratio of Ag and Tb is 4 : 1. After reaching peak intensity, the fluorescence intensity begins to decrease. This result
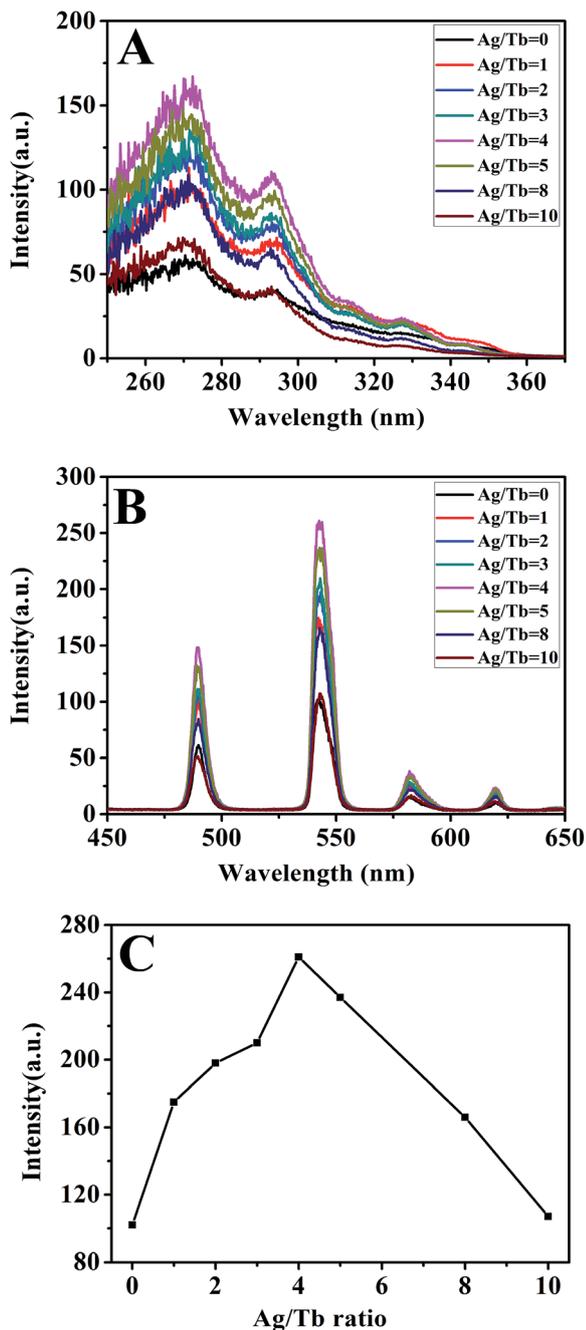
Fig. 6 (A) Excitation spectra (λ_{em} = 539 nm), (B) emission spectra (λ_{ex} = 294 nm) of Ag-NPs/Tb-complex/PLLA fibers with different Ag/Tb mole ratios and (C) a plot of fluorescence intensity against Ag/Tb mole ratios of the fibers.

confirms that Ag-NPs can enhance the fluorescence intensities of the Tb-complex/PLLA fibers. This positive effect is mainly attributed to LSPR of Ag-NPs. The LSPR effect on fluorescence property of fibers is illustrated in Fig. 7.

The intensity of LSPR can affect the fluorescence intensities of nearby rare earth ions.[23] A high degree of the space locality of the LSPR of Ag-NPs leads to more significant enhancement on the surrounding local electromagnetic field close to Ag-NPs.[31,32] The enhanced local electromagnetic field further leads to
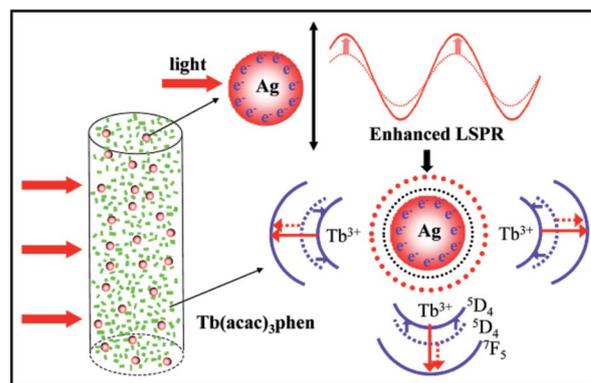

Fig. 7 Schematic diagram of LSPR effect on fluorescence of Tb^{3+} ions.

plasmonic interaction and also strongly affects the kinetic characteristics of nearby Tb-complex.[33] Furthermore, the radiative decay rates of the Tb^{3+} are also enhanced.[34] Meanwhile, the local field surrounding of Tb^{3+} ions is influenced. This has earlier been confirmed by the XPS analysis in Fig. 4. The change of local field surrounding further affects energy transfer between the ligands and Tb^{3+} ions and the resulting fluorescence intensity. As a result, the fluorescence intensity of fibers is greatly enhanced by Ag-NPs when the mole ratio of Ag/Tb is 4 : 1. However, when the Ag/Tb mole ratio further increases to 8 : 1, the intensity of the fibers decreases. The decrease in fluorescence intensity at a high concentration of Ag-NPs is attributed to the close distance between Ag-NPs and Tb-complex, and the resulting fluorescence quenching of Tb^{3+} ions.[22]

Fluorescence quantum efficiency represents the ability of fluorescence materials transforming the absorbing light energy into fluorescence. Table 1 illustrates that Ag-NPs/Tb-complex/PLLA fibers have higher quantum efficiency than the fibers without Ag-NPs when the Ag/Tb ratio is below 4. This increase in quantum efficiency is also caused by the LSPR effect of Ag-NPs. When the Ag/Tb ratio increases to 8, the quantum efficiency of Ag-NPs/Tb-complex/PLLA fibers is lower than the fibers without Ag-NPs, and this is attributed to the fluorescence quenching by the excess Ag-NPs.

Fig. 8 shows the curve of the fluorescence decay for Ag-NPs/Tb-complex/PLLA fibers. All of these curves could be well-fitted with the equation:

$$I = A + B\exp(-t/\tau)$$

where I is the relative fluorescence intensity; A and B are the fitting constants, respectively; t is the time; τ is fluorescence

Table 1 Quantum efficiencies (η) and lifetimes (τ) of Ag-NPs/Tb-complex/PLLA fibers with different Ag/Tb ratios

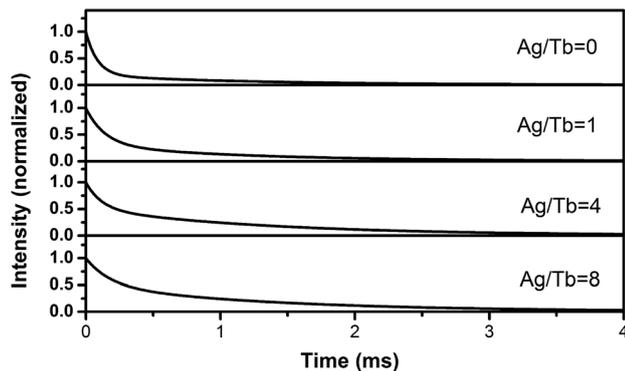| Samples	1# Ag/Tb = 0	2# Ag/Tb = 1	3# Ag/Tb = 4	4# Ag/Tb = 8
η (%)	12.1	15.3	21.5	9.6
τ (µs)	1744	4063	9098	8252

Paper

Fig. 8 Fluorescence decay curves of Ag-NPs/Tb-complex/PLLA fibers with different Ag/Tb ratios.

lifetime. The measured values of the fluorescence lifetime are listed in Table 1. The fluorescence lifetimes of all Ag-NPs/Tb-complex/PLLA fibers are higher than that of Tb-complex/PLLA fibers. According to the equation $\tau = 1/(A_{rad} + A_{nrad})$,[35] this enhancement of fluorescence lifetime is attributed to the decrease in the sum of the radiative transition rate (A_{rad}) and non-radiative transition rate (A_{nrad}). As A_{rad} is enhanced by the LSPR of Ag-NPs, the decrease in the A_{nrad} mainly contributes to the decrease in the sum of ($A_{rad} + A_{nrad}$) and the resulting long lifetime of Ag-NPs/Tb-complex/PLLA fibers.

Conclusions

This work mainly prepared Ag-NPs/Tb-complex/PLLA fibers by electrospinning, and researched the enhanced fluorescence properties of the composite fibers. The results showed that the fibers had smooth surfaces and diameters of around 250 nm. The Tb-complex dispersed uniformly in the PLLA fibers. With the addition of Ag-NPs, the local field surrounding environment of Tb^{3+} in the fibers was altered. Also, the LSPR effect of Ag-NPs influenced the energy transfer of Tb-complex, leading to an increase in fluorescence intensity of Ag-NPs/Tb-complex/PLLA fibers. Meanwhile, the addition of Ag-NPs improved quantum efficiency and extended fluorescence lifetime of Tb^{3+} in the composite fibers at the same time when the ratio of Ag/Tb was below 4.

Acknowledgements

Notes and references

1 M. C. Chen, Y. C. Sun and Y. H. Chen, *Acta Biomater.*, 2013, **9**, 5562–5572.

2 W. Liu, J. Wei, Y. Chen, P. Huo and Y. Wei, *ACS Appl. Mater. Interfaces*, 2013, **5**, 680–685.

3 Z. Hou, G. Li, H. Lian and J. Lin, *J. Mater. Chem.*, 2012, **22**, 5254.

4 S. N. Raja, A. C. Olson, K. Thorkelsson, A. J. Luong, L. Hsueh, G. Chang, B. Gludovatz, L. Lin, T. Xu, R. O. Ritchie and A. P. Alivisatos, *Nano Lett.*, 2013, **13**, 3915–3922.

5 X. P. Zhang, S. P. Wen, S. Hu, Q. Chen, H. Fong, L. Q. Zhang and L. Liu, *J. Phys. Chem. C*, 2010, **114**, 3898–3903.

6 Y. Lv, J. Wu, L. Wan and Z. Xu, *J. Phys. Chem. C*, 2008, **112**, 10609–10615.

7 B. Sun, Y. Z. Long, Z. J. Chen, S. L. Liu, H. D. Zhang, J. C. Zhang and W. P. Han, *J. Mater. Chem. C*, 2014, **2**, 1209–1219.

8 S. Wen, X. Zhang, L. Yao, M. Xi, L. Zhang, H. Fong and L. Liu, *J. Phys. Chem. C*, 2013, **1**, 1613.

9 X. Zhang, S. Wen, S. Hu, L. Zhang and L. Liu, *J. Rare Earths*, 2010, **28**, 333–339.

10 L. Huang, L. Cheng, H. Yu, J. Zhang, L. Zhou, J. Sun, H. Zhong, X. Li, Y. Tian, Y. Zheng, T. Yu, C. Li, H. Zhong, W. Liu, L. Zhang, J. Wang and B. Chen, *Opt. Commun.*, 2012, **285**, 1476–1480.

11 G. Gai, L. Wang, X. Dong and S. Xu, *J. Mater. Sci.*, 2013, **48**, 5140–5147.

12 C. F. Bohren and D. R. Huffman, *Absorption and Scattering of Light by Small Particles*, Wiley Interscience, 1983, vol. 98, pp. 290–291.

13 B. Sepúlveda, P. C. Angelomé, L. M. Lechuga and L. M. Liz-Marzán, *Nano Today*, 2009, **4**, 244–251.

14 X. Liao, Y. Chen, M. Qin, Y. Chen, L. Yang, H. Zhang and Y. Tian, *Talanta*, 2013, **117**, 203–208.

15 J. N. Anker, W. P. Hall, O. Lyandres, N. C. Shah, J. Zhao and R. P. V. Duyne, *Nat. Mater.*, 2008, **7**, 442–453.

16 R. Abargues, P. J. Rodriguez-Canto, S. Albert, I. Suarez and J. P. Martínez-Pastor, *J. Mater. Chem. C*, 2014, **2**, 908–915.

17 O. L. Malta and M. A. Couto dos Santos, *Chem. Phys. Lett.*, 1990, **174**, 13–18.

18 R. Reisfeld, T. Saraidarov, G. Panzer, V. Levchenko and M. Gaft, *Opt. Mater.*, 2011, **34**, 351–354.

19 M. Eichelbaum and K. Rademann, *Adv. Funct. Mater.*, 2009, **19**, 2045–2052.

20 G. P. Acuna, F. M. Moller, P. Holzmeister, S. Beater, B. Lalkens and P. Tinnefeld, *Science*, 2012, **338**, 506–510.

21 H. S. Wang, F. N. Xiao, Z. Q. Li, J. Ouyang, Z. Q. Wu, X. H. Xia and G. J. Zhou, *Lab Chip*, 2014, **14**, 1123–1128.

22 H. S. Wang, C. Wang, Y. K. He, F. N. Xiao, W. J. Bao, X. H. Xia and G. J. Zhou, *Anal. Chem.*, 2014, **86**, 3013–3019.

23 H. Li, M. Wang, W. Qiang, H. Hu, W. Li and D. Xu, *Analyst*, 2014, **139**, 1653–1660.

24 H. Lin, D. Chen, Y. Yu, R. Zhang and Y. Wang, *Appl. Phys. Lett.*, 2013, **103**, 091902.

25 T. Hayakawa, S. T. Selvan and M. Nogami, *J. Non-Cryst. Solids*, 1999, **259**, 16–22.

26 D. Zhang, X. Hu, R. Ji, S. Zhan, J. Gao, Z. Yan, E. Liu, J. Fan and X. Hou, *J. Non-Cryst. Solids*, 2012, **358**, 2788–2792.

27 X. Zong, K. Kim, D. Fang, S. Ran, H. S. Benjamin and C. Benjamin, *Polymer*, 2002, **43**, 4403–4412.

28 W. K. Son, J. H. Youk, T. S. Lee and W. H. Park, *Polymer*, 2004, **45**, 2959–2966.

29 J. Bai, Y. Li, S. Yang, J. Du, S. Wang, J. Zheng, Y. Wang, Q. Yang, X. Chen and X. Jing, *Solid State Commun.*, 2007, **141**, 292–295.

30 Y. S. Kawashima, C. F. Gugliotti, M. Yee, S. H. Tatumi and J. C. R. Mittani, *Radiat. Phys. Chem.*, 2014, **95**, 91–93.

31 N. Calander and M. Willander, *J. Appl. Phys.*, 2002, **92**, 4878–4884.

32 P. Muhlschlegel, H. J. Eisler, O. J. Martin, B. Hecht and D. W. Pohl, *Science*, 2005, **308**, 1607–1609.

33 C. Mihalcea, D. Büchel, N. Atoda and J. Tominaga, *J. Am. Chem. Soc.*, 2001, **123**, 7172–7173.

34 W. Ji, P. Jing and J. Zhao, *J. Mater. Chem. C*, 2013, **1**, 470–476.

35 A. K. Bansal, A. Ruseckas, P. E. Shaw and I. D. W. Samuel, *J. Phys. Chem. C*, 2010, **114**, 17864–17867.